Numerical simulation of laminar incompressible fluid-structure interaction for elastic material with point constraints

M. Razzaq[1], J. Hron[2] and S. Turek[3]

[1] Institute of Applied Mathematics, TU Dortmund, Germany.
mrazzaq@math.uni-dortmund.de
[2] Institute of Mathematics, Charles University, Czech Republic.
hron@karlin.mff.cuni.cz
[3] Institute of Applied Mathematics, TU Dortmund, Germany.
ture@featflow.de

Summary. We present numerical techniques for solving the problem of fluid structure interaction with a compressible elastic material in a laminar incompressible viscous flow via fully coupled monolithic Arbitrary Lagrangian-Eulerian (ALE) formulation. The mathematical description and the numerical schemes are designed in such a way that more complicated constitutive relations can be easily incorporated. The whole domain of interest is treated as one continuum and we utilize the well known Q_2P_1 finite element pair for discretization in space to gain high accuracy. We perform numerical comparisons for different time stepping schemes, including variants of the Fractional-Step-θ-scheme, Backward Euler and Crank-Nicholson scheme for both solid and fluid parts. The resulting nonlinear discretized algebraic system is solved by a quasi-Newton method which approximates the Jacobian matrices by the divided differences approach and the resulting linear systems are solved by a geometric multigrid approach. In the numerical examples, a cylinder with attached flexible beam is allowed to freely rotate around its axis which requires a special numerical treatment. By identifying the center of the cylinder with one grid point of the computational mesh we prescribe a Dirichlet type boundary condition for the velocity and the displacement of the structure at this point, which allows free rotation around this point. We present numerical studies for different problem parameters on various mesh types and compare the results with experimental values from a corresponding benchmarking experiment.

1 Introduction

We consider the problem of viscous fluid flow interacting with an elastic body which is being deformed by the fluid action. Such a problem is encountered in many real life applications of great importance. Typical examples of this type of problem are the areas of biomedical fluids which include joint lubrication and deformable cartilage and blood flow interaction with

implants. The theoretical investigation of fluid structure interaction problems is complicated by the need of a mixed description. While for the solid part the natural view is the material (Lagrangian) description, for the fluid it is the spatial (Eulerian) description. In the case of their combination some kind of mixed description (usually referred to as the Arbitrary Lagrangian-Eulerian description or ALE) has to be used which brings additional nonlinearity into the resulting equations.

A numerical solution of the resulting equations of the fluid structure interaction problem poses great challenges since it includes the features of elasticity, fluid mechanics and their coupling. The easiest solution strategy, mostly used in the available software packages, is to decouple the problem into the fluid part and solid part, for each of those parts using some well established method of solution; then the interaction process is introduced as external boundary conditions in each of the subproblems. This has the advantage that there are many well tested numerical methods for both separate problems of fluid flow and elastic deformation, while on the other hand the treatment of the interface and the interaction is problematic. In contrast, the approach presented here treats the problem as a single continuum with the coupling automatically taken care of as internal interface, which in our formulation does not require any special treatment.

2 Fluid-structure interaction problem formulation

A general fluid structure interaction problem consists of the description of the fluid and solid fields, appropriate interface conditions at the interface and conditions for the remaining boundaries, respectively. In this paper, we consider the flow of an incompressible Newtonian fluid interacting with an elastic solid. We denote the domain occupied by the fluid by Ω_t^f and the solid by Ω_t^s at the time $t \in [0,T]$. Let $\Gamma_t^0 = \bar{\Omega}_t^f \cap \bar{\Omega}_t^s$ be the part of the boundary where the elastic solid interacts with the fluid.

In the following, the fields and interface conditions are introduced. Furthermore, problem configurations and solution procedure for each of the fields is presented in detail.

2.1 Fluid

The fluid is considered to be **Newtonian**, **incompressible** and its state is described by the *velocity* and *pressure* fields $\mathbf{v}^f$, p^f respectively. The constant density of the fluid is ρ^f and the kinematic viscosity is denoted by ν^f. The balance equations are:

$$\rho^f \frac{D\mathbf{v}^f}{Dt} = \operatorname{div} \sigma^f, \quad \operatorname{div} \mathbf{v}^f = 0 \quad \text{in} \quad \Omega_t^f \tag{1}$$

In order to solve the balance equations we need to specify the constitutive relations for the stress tensors. For the fluid we use the incompressible Newtonian relation

$$\sigma^f = -p^f \mathbf{I} + \mu(\nabla \mathbf{v}^f + (\nabla \mathbf{v}^f)^T), \tag{2}$$

where μ represents the dynamic viscosity of the fluid and p^f is the Lagrange multiplier corresponding to the incompressibility constraint in (1). The material time derivative depends on the choice of the reference system. There are basically 3 alternative reference systems: the Eulerian, the Lagrangian, and the Arbitrary Lagrangian Eulerian formulation. The most commonly used description for the fluid structure interaction is the ALE description. For the ALE formulation presented in this paper, discretization techniques are discussed in section 3.

2.2 Structure

The structure is assumed to be **elastic** and **compressible**. Its configuration is described by the displacement $\mathbf{u^s}$, with velocity field $\mathbf{v^s} = \frac{\partial \mathbf{u}^s}{\partial t}$. The balance equations are:

$$\rho^s \frac{\partial \mathbf{v}^s}{\partial t} + \rho^s (\nabla \mathbf{v}^s)\mathbf{v}^s = \operatorname{div} \sigma^s + \rho^s \mathbf{g}, \quad \text{in} \quad \Omega_t^s. \tag{3}$$

Written in the more common Lagrangian description, i.e. with respect to some fixed reference (initial) state Ω^s, we have

$$\rho^s \frac{\partial^2 \mathbf{u^s}}{\partial t^2} = \operatorname{div}(J\sigma^s F^{-T}) + \rho^s \mathbf{g}, \quad \text{in} \quad \Omega^s. \tag{4}$$

The constitutive relations for the stress tensors for the compressible structure are presented, however, also incompressible structures can be handled in the same way. The density of the structure in the undeformed configuration is ρ^s. The material elasticity is characterized by a set of two parameters, the Poisson ratio ν^s and the Young modulus E. Alternatively, the characterization is described by the Lam*é* coefficients λ^s and the shear modulus μ^s. These parameters satisfy the following relations

$$\nu^s = \frac{\lambda^s}{2(\lambda^s + \mu^s)} \qquad E = \frac{\mu^s(3\lambda^s + 2\mu^2)}{(\lambda^s + \mu^s)} \tag{5}$$

$$\mu^s = \frac{E}{2(1+\nu^s)} \quad \lambda^s = \frac{\nu^s E}{(1+\nu^s)(1-2\nu^s)}, \tag{6}$$

where $\nu^s = 1/2$ for a incompressible and $\nu^s < 1/2$ for a compressible structure. In the large deformation case it is common to describe the constitutive equation using a stress-strain relation based on the Green Lagrangian strain tensor E and the 2.Piola-Kirchhoff stress tensor $S(E)$ as a function of E. The 2.Piola-Kirchhoff stress can be obtained from the Cauchy stress σ^s as

$$S^s = JF^{-1}\sigma^s F^{-T}, \tag{7}$$

and the Green-Lagrange tensor E as

$$E = \frac{1}{2}(F^T F - I). \tag{8}$$

In this paper, the material is specified by giving the Cauchy stress tensor σ^s by the following constitutive law for the **St.Venant-Kirchhoff material** for simplicity

$$\sigma^s = \frac{1}{J}\mathbf{F}(\lambda^s(trE)I + 2\mu^s E)\mathbf{F}^T \qquad \mathbf{S}^s = \lambda^s(trE)I + 2\mu^s E. \tag{9}$$

J denotes the determinant of the deformation gradient tensor F, defined as $F = I + \nabla \mathbf{u^s}$.

2.3 Interaction Condition

The boundary conditions on the fluid solid interface are assumed to be

$$\sigma^f n = \sigma^s n, \quad \mathbf{v}^f = \mathbf{v}^s, \quad \text{on} \quad \Gamma_t^0, \tag{10}$$

where n is a unit normal vector to the interface Γ_t^0. This implies the no-slip condition for the flow and that the forces on the interface are in balance.

3 Discretization and solution techniques

The common solution approach is a separate discretization in space and time. We first discretize in time by one of the usual methods known from the treatment of ordinary differential equations, such as the Backward Euler (BE), the Crank-Nicholson (CN), Fractional-Step-θ-scheme (FS) or a new modified Fractional-Step-θ-scheme (GL). Properties of these time stepping schemes applying on incompressible Navier-Stokes equations are described in detail below.

3.1 Time discretization

We consider numerical solution techniques for the incompressible Navier-Stokes equations

$$\mathbf{v}_t - \nu\Delta\mathbf{v} + \mathbf{v}\cdot\nabla\mathbf{v} + \nabla p = \mathbf{f}, \quad \mathrm{div}\,\mathbf{v} = 0, \quad \text{in} \quad \Omega\times(0,T], \tag{11}$$

for given force $\mathbf{f}$ and viscosity ν, with prescribed boundary values on the boundary $\partial\Omega$ and an initial condition at $t = 0$.

Basic θ-scheme

Given $\mathbf{v}^n$ and $K = t_{n+1} - t_n$, then solve for $\mathbf{v} = \mathbf{v}^{n+1}$ and $p = p^{n+1}$

$$\frac{\mathbf{v}-\mathbf{v}^n}{K} + \theta[-\nu\Delta\mathbf{v} + \mathbf{v}\cdot\nabla\mathbf{v}] + \nabla p = \mathbf{g}^{n+1}, \quad \mathrm{div}\,\mathbf{v} = 0, \quad \text{in} \quad \Omega \tag{12}$$

with right hand side $\mathbf{g}^{n+1} := \theta\mathbf{f}^{n+1} + (1-\theta)\mathbf{f}^n - (1-\theta)[-\nu\Delta\mathbf{v}^n + \mathbf{v}^n\cdot\nabla\mathbf{v}^n]$.

The parameter θ has to be chosen depending on the time-stepping scheme, e.g., $\theta = 1$ for the Backward Euler, or $\theta = 1/2$ for the Crank-Nicholson-scheme. The pressure term $\nabla p = \nabla p^{n+1}$ may be replaced by $\theta\nabla p^{n+1} + (1-\theta)\nabla p^n$, but, with appropriate postprocessing, both strategies lead to solutions of the same accuracy. In all cases, we end up with the task of solving, at each time step, a nonlinear saddle point problem of given type which has then to be discretized in space.

In the past, explicit time-stepping schemes have been commonly used in nonstationary flow calculations, but because of the severe stability problems inherent in this approach, the required small time steps prohibit the efficient treatment of long time flow simulations. Due to the high stiffness, one should prefer implicit schemes in the choice of time-stepping methods for solving this problem. Since implicit methods have become feasible thanks to more efficient nonlinear and linear solvers, the schemes most frequently used are still either the simple first-order Backward Euler scheme (BE), with $\theta = 1$, or more preferably the second-order Crank-Nicholson scheme (CN), with $\theta = 1/2$.

These two methods belong to the group of *One-Step-θ-schemes*. The CN scheme occasionally suffers from numerical instabilities because of its only weak damping property (not strongly A-stable), while the BE-scheme is of first order accuracy only (however: it is a good candidate for steady-state simulations). Another method which has proven to have the potential to excel

in this competition is the Fractional-Step-θ-scheme (FS). It uses three different values for θ and for the time step K at each time level.

We define a time step with $K = t_{n+1} - t_n$ in the case of the Backward Euler or the Crank-Nicholson scheme, with the same θ ($\theta = 0.5$ or $\theta = 1$) as above. In the following, we use the more compact form for the diffusive and advective part:

$$N(\mathbf{v})\mathbf{v} = -\nu\Delta\mathbf{v} + \mathbf{v}\cdot\nabla\mathbf{v} \tag{13}$$

Backward Euler-scheme

$$\begin{aligned} [I + KN(\mathbf{v}^{n+1})]\mathbf{v}^{n+1} + \nabla p^{n+1} &= \mathbf{v}^n + K\mathbf{f}^{n+1} \\ \operatorname{div}\mathbf{v}^{n+1} &= 0 \end{aligned}$$

Crank-Nicholson-scheme

$$\begin{aligned} [I + \tfrac{K}{2}N(\mathbf{v}^{n+1})]\mathbf{v}^{n+1} + \nabla p^{n+1} &= [I - \tfrac{K}{2}N(\mathbf{v}^n)]\mathbf{v}^n + \tfrac{K}{2}\mathbf{f}^{n+1} + \tfrac{K}{2}\mathbf{f}^n \\ \operatorname{div}\mathbf{v}^{n+1} &= 0 \end{aligned}$$

Fractional-Step-θ-scheme

For the Fractional-Step-θ-scheme we proceed as follows. Choosing $\theta = 1 - \frac{\sqrt{2}}{2}$, $\theta' = 1 - 2\theta$, and $\alpha = \frac{1-2\theta}{1-\theta}$, $\beta = 1 - \alpha$, the macro time step $t_n \to t_{n+1} = t_n + K$ is split into the three following consecutive sub steps (with $\tilde{\theta} := \alpha\theta K = \beta\theta' K$):

$$\begin{aligned} [I + \tilde{\theta}N(\mathbf{v}^{n+\theta})]\mathbf{v}^{n+\theta} + \nabla p^{n+\theta} &= [I - \beta\theta KN(\mathbf{v}^n)]\mathbf{v}^n + \theta K\mathbf{f}^n \\ \operatorname{div}\mathbf{v}^{n+\theta} &= 0 \end{aligned}$$

$$\begin{aligned} [I + \tilde{\theta}N(\mathbf{v}^{n+1-\theta})]\mathbf{v}^{n+1-\theta} + \nabla p^{n+1-\theta} &= [I - \alpha\theta' KN(\mathbf{v}^{n+\theta})]\mathbf{v}^{n+\theta} \\ &\quad + \theta' K\mathbf{f}^{n+1-\theta} \\ \operatorname{div}\mathbf{v}^{n+1-\theta} &= 0 \end{aligned}$$

$$\begin{aligned} [I + \tilde{\theta}N(\mathbf{v}^{n+1})]\mathbf{v}^{n+1} + \nabla p^{n+1} &= [I - \beta\theta KN(\mathbf{v}^{n+1-\theta})]\mathbf{v}^{n+1-\theta} \\ &\quad + \theta K\mathbf{f}^{n+1-\theta} \\ \operatorname{div}\mathbf{v}^{n+1} &= 0 \end{aligned}$$

A modified Fractional-Step-θ-scheme

Consider an initial value problem of the following form, with $X(t) \in \mathbf{R}^d, d \geq 1$:

$$\begin{cases} \dfrac{dX}{dt} &= f(X,t) \quad \forall t > 0 \\ X(0) &= X_0 \end{cases} \tag{14}$$

Then, a modified θ-scheme (see [7] and [8]) with macro time step Δt can be written again as three consecutive sub steps, where $\theta = 1-1/\sqrt{2}$, $X^0 = X_0$, $n \geq 0$ and X^n is known:

$$\begin{aligned} \frac{X^{n+\theta} - X^n}{\theta \Delta t} &= f\left(X^{n+\theta}, t^{n+\theta}\right) \\ X^{n+1-\theta} &= \frac{1-\theta}{\theta} X^{n+\theta} + \frac{2\theta - 1}{\theta} X^n \\ \frac{X^{n+1} - X^{n+1-\theta}}{\theta \Delta t} &= f\left(X^{n+1}, t^{n+1}\right) \end{aligned}$$

As shown in [8], the most important properties of this θ-scheme are that

- it is fully implicit;
- it is strongly A-stable;
- it is second order accurate (in fact, it is "nearly" third order accurate [8]).

These properties promise some advantageous behavior, particularly in implicit CFD simulations for nonstationary incompressible flow problems. Applying one step of this scheme to the Navier-Stokes equations, we obtain the following variant of the scheme:

1. $$\begin{cases} \dfrac{\mathbf{v}^{n+\theta} - \mathbf{v}^n}{\theta \Delta t} + N(\mathbf{v}^{n+\theta})\mathbf{v}^{n+\theta} + \nabla p^{n+\theta} = \mathbf{f}^{n+\theta} \\ \operatorname{div} \mathbf{v}^{n+\theta} = 0 \end{cases}$$

2. $$\mathbf{v}^{n+1-\theta} = \tfrac{1-\theta}{\theta}\mathbf{v}^{n+\theta} + \tfrac{2\theta-1}{\theta}\mathbf{v}^n$$

3. $$\begin{cases} \dfrac{\mathbf{v}^{n+1} - \mathbf{v}^{n+1-\theta}}{\theta \Delta t} + N(\mathbf{v}^{n+1})\mathbf{v}^{n+1} + \nabla \widetilde{p}^{n+1} = \mathbf{f}^{n+1} \\ \operatorname{div} \mathbf{v}^{n+1} = 0 \end{cases}$$

3*b*. $$p^{n+1} = (1-\theta)p^{n+\theta} + \theta \widetilde{p}^{n+1}$$

These 3 substeps build one macro time step and have to be compared with the previous description of the Backward Euler, Crank-Nicholson and the classical Fractional-Step-θ-scheme which all have been formulated in terms of a macro time step with 3 sub steps, too. Then, the resulting accuracy and numerical cost are better comparable and the rating is fair. The main difference to the previous 'classical' FS scheme is that substeps 1. and 3. look like a Backward Euler step while substep 2. is an extrapolation step only for previously computed data such that no operator evaluations at previous time steps are required.

Substep 3b. can be viewed as postprocessing step for updating the new pressure which however is not a must. In fact, in our numerical tests [7] we omitted this substep 3b. and accepted the pressure from substep 3. as final pressure approximation, that means $p^{n+1} = \widetilde{p}^{n+1}$.

Summarizing, one obtains that the numerical effort of the modified scheme for each substep is cheaper - at least for 'small' time steps (treatment of the nonlinearity) and complex right hand side evaluations while the resulting accuracy is similar. Incidentally, the modified θ-scheme is a *Runge-Kutta* one; it has been derived in [8] as a particular case of the Fractional-Step-θ-scheme.

3.2 Space discretization

Our treatment of the fluid structure-interaction problem as one system suggests that we use the same finite elements for both the solid part and the fluid region. Since the fluid is incompressible we have to choose a pair of finite element spaces known to be stable for problems with incompressibility constraint.

The conforming element Q_2P_1

One possible choice is the conforming biquadratic, discontinuous linear Q_2P_1 pair, see figure 1 for the location of the degrees of freedom. This choice results in 39 degrees of freedom per element in the case of displacement, velocity, pressure formulation in two dimensions and 112 degrees of freedom per element in three dimensions. Let us define the following spaces

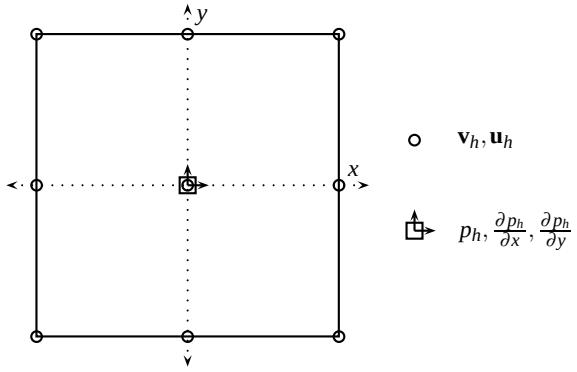

Fig. 1. Location of the degrees of freedom for the Q_2P_1 element.

$$
\begin{aligned}
U &= \{\mathbf{u} \in L^\infty(I,[W^{1,2}(\Omega)]^3), \mathbf{u} = \mathbf{0} \text{ on } \partial\Omega\},\\
V &= \{\mathbf{v} \in L^2(I,[W^{1,2}(\Omega_t)]^3) \cap L^\infty(I,[L^2(\Omega_t)]^3), \mathbf{v} = \mathbf{0} \text{ on } \partial\Omega\},\\
P &= \{p \in L^2(I,L^2(\Omega))\},
\end{aligned}
$$

then the variational formulation of the fluid-structure interaction problem is to find $(\mathbf{u},\mathbf{v},p) \in U \times V \times P$ such that the equations are satisfied for all $(\zeta,\xi,\gamma) \in U \times V \times P$ including appropriate initial conditions. The spaces U,V,P on an interval $[t^n,t^{n+1}]$ would be approximated in the case of the Q_2,P_1 pair as

$$
\begin{aligned}
U_h &= \{\mathbf{u}_h \in [C(\Omega_h)]^2, \mathbf{u}_h|_T \in [Q_2(T)]^2 \quad \forall T \in \mathscr{T}_h, \mathbf{u}_h = \mathbf{0} \text{ on } \partial\Omega\},\\
V_h &= \{\mathbf{v}_h \in [C(\Omega_h)]^2, \mathbf{v}_h|_T \in [Q_2(T)]^2 \quad \forall T \in \mathscr{T}_h, \mathbf{v}_h = \mathbf{0} \text{ on } \partial\Omega\},\\
P_h &= \{p_h \in L^2(\Omega_h), p_h|_T \in P_1(T) \quad \forall T \in \mathscr{T}_h\}.
\end{aligned}
$$

Let us denote by $\mathbf{u}_h^n$ the approximation of $\mathbf{u}(t^n)$, $\mathbf{v}_h^n$ the approximation of $\mathbf{v}(t^n)$ and p_h^n the approximation of $p(t^n)$. Consider for each $T \in T_h$ the bilinear transformation $\psi_T : \hat{T} \to T$ to the unit square T. Then, $Q_2(T)$ is defined as

$$\mathrm{Q}_2(T) = \left\{ q \circ \psi_T^{-1} : q \in span < 1, x, y, xy, x^2, y^2, x^2y, y^2x, x^2y^2 > \right\} \tag{15}$$

with nine local degrees of freedom located at the vertices, midpoints of the edges and in the center of the quadrilateral. The space $P_1(T)$ consists of linear functions defined by

$$\mathrm{P}_1(T) = \left\{ q \circ \psi_T^{-1} : q \in span < 1, x, y > \right\} \tag{16}$$

with the function value and both partial derivatives located in the center of the quadrilateral, as its three local degrees of freedom, which leads to a discontinuous pressure. The inf-sup condition is satisfied (see [2]); however, the combination of the bilinear transformation ψ with a linear function on the reference square $P_1(\widehat{T})$ would imply that the basis on the reference square did not contain the full basis. So, the method can at most be first order accurate on general meshes (see [1, 2])

$$\|p - p_h\| = O(h). \tag{17}$$

The standard remedy is to consider a local coordinate system (ξ, η) obtained by joining the midpoints of the opposing faces of T (see [1, 5, 6]). Then, we set on each element T

$$P_1(T) := span < 1, \xi, \eta > . \tag{18}$$

For this case, the inf-sup condition is also satisfied and the second order approximation is recovered for the pressure as well as for the velocity gradient (see [2, 3])

$$\|p - p_h\| = O(h^2) \quad \text{and} \quad \|\nabla(u - u_h)\|_0 = O(h^2). \tag{19}$$

For a smooth solution, the approximation error for the velocity in the L_2-norm is of order $O(h^3)$ which can easily be demonstrated for prescribed polynomials or for smooth data on appropriate domains.

3.3 Solution algorithm

The system of nonlinear algebraic equations arising from the governing equations prescribed in section 2.1 and 2.2 is

$$\begin{bmatrix} S_{\mathbf{uu}} & S_{\mathbf{uv}} & 0 \\ S_{\mathbf{vu}} & S_{\mathbf{vv}} & kB \\ c_{\mathbf{u}} B_s^T & c_{\mathbf{v}} B_f^T & 0 \end{bmatrix} \begin{bmatrix} \mathbf{u} \\ \mathbf{v} \\ p \end{bmatrix} = \begin{bmatrix} \mathbf{f_u} \\ \mathbf{f_v} \\ f_p \end{bmatrix} \tag{20}$$

which is typical saddle point problem, where S describes the diffusive and convective terms from the governing equations. The above system of nonlinear algebraic equations (20) is solved using Newton method as basic iteration. The basic idea of the Newton iteration is to find a root of a function, $\mathbf{R}(\mathbf{X}) = \mathbf{0}$, using the available known function value and its first derivative, where $\mathbf{X} = (\mathbf{u}_h, \mathbf{v}_h, p_h) \in U_h \times V_h \times P_h$. One step of the Newton iteration can be written as

$$\mathbf{X}^{n+1} = \mathbf{X}^n - \left[\frac{\partial \mathbf{R}}{\partial \mathbf{X}} (\mathbf{X}^n) \right]^{-1} \mathbf{R}(\mathbf{X}^n). \tag{21}$$

1. Let $\mathbf{X}^n$ be some starting guess.
2. Set the residuum vector $\mathbf{R}^n = \mathbf{R}(\mathbf{X}^n)$ and the tangent matrix $\mathbf{A} = \frac{\partial \mathbf{R}}{\partial \mathbf{X}}(\mathbf{X}^n)$.
3. Solve for the correction $\delta\mathbf{X}$
$$\mathbf{A}\delta\mathbf{X} = \mathbf{R}^n.$$
4. Find optimal step length ω.
5. Update the solution $\mathbf{X}^{n+1} = \mathbf{X}^n - \omega\delta\mathbf{X}$.

Fig. 2. One step of the Newton method with line search.

This basic iteration can exhibit quadratic convergence provided that the initial guess is sufficiently close to the solution. To ensure the convergence globally, some improvements of this basic iteration are used. The damped Newton method with line search improves the chance of convergence by adaptively changing the length of the correction vector. The solution update step in the Newton method (21) is replaced by

$$\mathbf{X}^{n+1} = \mathbf{X}^n - \omega\delta\mathbf{X}, \tag{22}$$

where the parameter ω is determined such that a certain error measure decreases (see [6, 15] for more details). The Jacobian matrix $\frac{\partial \mathbf{R}(\mathbf{X}^n)}{\partial \mathbf{X}}$ can be computed by finite differences from the residual vector $\mathbf{R}(\mathbf{X})$

$$\left[\frac{\partial \mathbf{R}}{\partial \mathbf{X}}\right]_{ij}(\mathbf{X}^n) \approx \frac{[\mathbf{R}]_i(\mathbf{X}^n + \alpha_j \mathbf{e}_j) - [\mathbf{R}]_i(\mathbf{X}^n - \alpha_j \mathbf{e}_j)}{2\alpha_j}, \tag{23}$$

where $\mathbf{e}_j$ are the unit basis vectors in $\mathbb{R}^n$ and the coefficients α_j are adaptively taken according to the change in the solution in the previous time step. Since we know the sparsity pattern of the Jacobian matrix in advance, which is given by the used finite element method, this computation can be done in an efficient way so that the linear solver remains the dominant part in terms of the CPU time (see [6, 14] for more details).

3.4 Multigrid solver

The solution of the linear problems is the most time consuming part of the solution process. A good candidate seems to be a direct solver for sparse systems like UMFPACK (see [11]); while this choice provides very robust linear solvers, its memory and CPU time requirements are too high for larger systems (i.e. more than 20.000 unknowns). Large linear problems can be solved by Krylov space methods (BiCGStab, GMRes, see [10]) with suitable preconditioners. One possibility is the ILU preconditioner with special treatment of the saddle point character of our system, where we allow certain fill-in for the zero diagonal blocks, see [13]. The alternative option for larger systems is the multigrid method presented in this section.

We also utilize a standard geometric multigrid approach based on a hierarchy of grids obtained by successive regular refinement of a given coarse mesh. The complete multigrid iteration is performed in the standard defect-correction setup with the V or F-type cycle. While a direct sparse solver [11] is used for the coarse grid solution, on finer levels a fixed number (2 or 4) of iterations by local MPSC schemes (Vanka-like smoother) [6, 12, 15] is performed. Such iterations can be written as

$$\begin{bmatrix} \mathbf{u}^{l+1} \\ \mathbf{v}^{l+1} \\ p^{l+1} \end{bmatrix} = \begin{bmatrix} \mathbf{u}^{l} \\ \mathbf{v}^{l} \\ p^{l} \end{bmatrix} - \omega \sum_{\text{element}\Omega_i} \begin{bmatrix} S_{\mathbf{uu}|\Omega_i} & S_{\mathbf{uv}|\Omega_i} & 0 \\ S_{\mathbf{vu}|\Omega_i} & S_{\mathbf{vv}|\Omega_i} & kB_{|\Omega_i} \\ c_{\mathbf{u}}B^T_{s|\Omega_i} & c_{\mathbf{v}}B^T_{f|\Omega_i} & 0 \end{bmatrix}^{-1} \begin{bmatrix} \mathbf{def}^l_{\mathbf{u}} \\ \mathbf{def}^l_{\mathbf{v}} \\ def^l_p \end{bmatrix}.$$

The inverse of the local systems (39×39) can be done by hardware optimized direct solvers. The full nodal interpolation is used as the prolongation operator $\mathbf{P}$ with its transposed operator used as the restriction $\mathbf{R} = \mathbf{P}^T$ (see [4, 6] for more details).

4 Objectives and problem configuration

The main objective of the following numerical investigation is to analyze and to validate our monolithic approach for a configuration with a point constraint ("rigid solid with rotational degree of freedom") for a special experimental set up. In the future, these numerical and experimental studies shall lead to a reliable data basis for the validation and comparison purposes of different numerical methods and code implementations for fluid-structure interaction simulations. These numerical studies are focused on the two-dimensional periodical swiveling motion of a simple flexible structure driven by a prescribed inflow velocity (see [9]). The structure has a linear mechanical behavior and the fluid is considered incompressible and in the laminar regime. The cylinder is fixed only at the center and can rotate freely. To allow for this kind of additional rotational movement in our method, the cylinder has to be included in the mesh in our recent approach. By prescribing zero displacement for the node located in the center of the cylinder we eliminate the translational degree of freedom of the whole structure but preserve the rotational freedom of the cylinder. Hence, the position of all other nodes located inside the cylinder are taken into account as part of the solution. We divided the numerical tests into two parts corresponding to the thickness of the elastic beam i.e for $1mm$ thick beam and for $0.04mm$ thick beam attached to an aluminum cylinder. At the trailing edge of the elastic beam a rectangular stainless steel mass is located. Both the rear mass and the cylinder are considered rigid. All the structure is free to rotate around an axis located in the center point of the cylinder. The detailed dimensions of the structure are presented in Fig. 3. The densities of the different materials used in the construction of the model are given in Table 1. The shear modulus of stainless steel is $7.58 \times 10^{13} kg/mms^2$ and Poisson ratio of the beam ν^p is taken as 0.3. The Young modulus is measured to be $200kN/mm^2$. As fluid for the tests, a

Table 1. Density values of the structure components.

Cylinder	(aluminum)	$2.828 \times 10^{-6} kg/mm^3$
Beam	(stainless steel)	$7.855 \times 10^{-6} kg/mm^3$
Rear mass	(stainless steel)	$7.800 \times 10^{-6} kg/mm^3$

Polyethylene glycol syrup is chosen because of its high viscosity and a density close to water. It has a kinematic viscosity $164mm^2/s$ and the density of the fluid is $1.05 \times 10^{-6} kg/mm^3$.

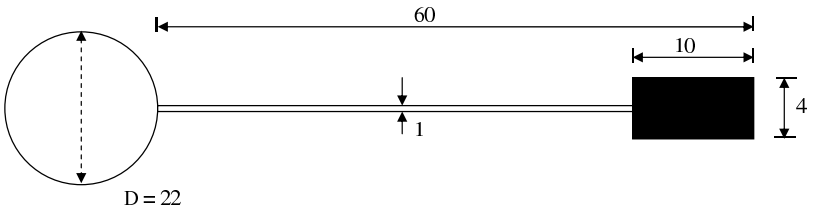

Fig. 3. Structure (dimensions in millimeters).

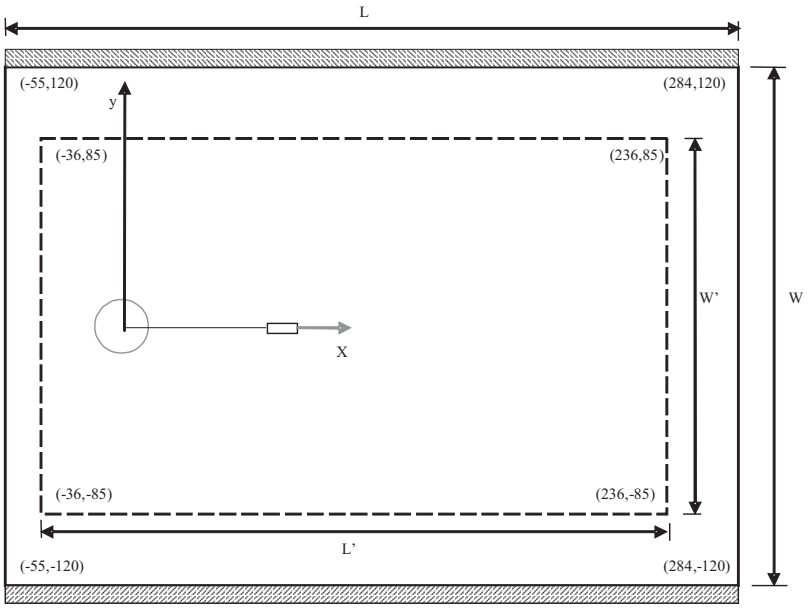

Fig. 4. Physical domain (continuous line) and flow field measuring domain (hatched line).

Geometry of the problem

The geometry of the physical domain coincides with the shape of the facility test function. The co-ordinate system used is centered in the rotating axis of the flexible structure front body. The x-axis is aligned with the incoming flow. Then, the geometric details are as follows:

• The overall dimensions of the physical domain are length $L = 338mm$ and width $W = 240mm$.

• The center of the cylindrical front body is C which is located 55mm downstream of the beginning of the physical domain, and the radius r is 11mm.

• The dimensions of the flow field measuring domain (hatched line) are given by length $L' = 272mm$ and width $W' = 170mm$. The measuring domain begins 19mm after the beginning of the physical domain as shown in Figure 4. The Reynolds number is defined by $Re = \frac{2rV}{v'}$

with mean velocity $\bar{\mathbf{V}} = \frac{2}{3}v(0,W/2,t)$, r radius of the cylinder and W height of the channel (see Fig. 4).

Boundary and Initial conditions

The velocity profile prescribed at the left channel inflow is defined as approximation of the experimental inflow data

$$\mathbf{v}^f(0,y) = \bar{U}(1-(y/120)^8)(1+(y/120)^8), \tag{24}$$

such that the maximum of the inflow velocity profile is $\bar{U}$. The outflow condition effectively prescribes some reference value for the pressure variable p. While this value could be arbitrarily set in the incompressible case, in the case of a compressible structure this will have influence onto the stress and consequently the deformation of the solid. The *no-slip* condition is prescribed for the fluid on the other boundary parts, i.e. top and bottom wall, circle and fluid-structure interface Γ_t^0. Suggested starting procedure for the non-steady tests is to use a smooth increase of the velocity profile in time as

$$\mathbf{v}^f(t,0,y) = \begin{cases} \mathbf{v}^f(0,y)\dfrac{1-cos(\pi t/2)}{2} & if \quad t<1 \\ \mathbf{v}^f(0,y) & \text{otherwise} \end{cases} \tag{25}$$

where $\mathbf{v}^f(0,y)$ is the velocity profile given in (24). Since the cylinder is allowed to freely rotate around its axis, we need to incorporate this into our setup. As described before, by identifying the center of the cylinder with one grid point of our mesh we can prescribe a Dirichlet type boundary condition for the velocity and the displacement of the structure at this point. This point constraint effectively fixes the position of the cylinder axis, but still allows the free rotation around this point.

5 Experimental results

Experimental studies on reference test cases were conducted in laminar flows ($Re \leq 200$) at the Institute of Fluid Mechanics at University of Erlangen-Nürnberg (see [9]). The structure was defined to be constituted by a $0.04mm$ thick stainless steel sheet attached to an $22mm$ diameter aluminum cylindrical front body. At the trailing edge of the beam a $10mm \times 4mm$ rectangular stainless steel mass was located. All the structure was free to rotate around an axis located in the center point of the front cylinder. Both the front cylinder and the rear mass were considered rigid. The structure model was tested in a viscous liquid flow at different velocities up to $2000mm/s$. The minimum velocity needed for the movement of the structure slightly varied from test to test. In most of the cases it was already possible to achieve a consistent swiveling motion for velocities slightly smaller than $1000mm/s$. The frequency of the structure movement increased linearly with the velocity of the approaching fluid. For velocity ranging from $1140mm/s$ to $1300mm/s$, the frequency of oscillations showed a pronounced hysteresis depending on increasing versus decreasing flow velocity. There were two test cases performed using different flow velocity and the corresponding results were as follows: Using velocity $1080mm/s$ ($Re \approx 145$) one measures a frequency of oscillations of the structure $\approx 6Hz$, and

with velocity $1450mm/s$ $(Re \approx 195)$ a frequency of oscillations of the structure $\approx 13.58Hz$ is observed. At higher velocities the motion of the structure became faster and more complex. At around $1300mm/s$ the structure shifted abruptly to a new swiveling mode in which the second deflection mode played an important role.

6 Numerical investigations

In this section we will present numerical results for the $1mm$ thick beam and preliminary calculations for the $0.04mm$ thick beam.

6.1 Results for 1mm thick beam

Experimental studies are conducted taking a $0.04mm$ thick beam. However, in the first numerical test we set the thickness of the beam $1mm$ (see Fig. 3) and also we reduce the rigidity of the beam (i.e., shear modulus) from $7.69 \times 10^7 kg/mms^2$ to $7.69 \times 10^4 kg/mms^2$ to make the problem numerically easier, all other parameters are from table 1. We applied the presented time stepping schemes, namely (BE, CN, FS, GL) prescribed in section 3.1 to analyze the behavior for different Δt. For $\Delta t = 0.0005$ almost the identical amplitude of oscillations (≈ 13.84) of rear mass is observed (see figure 7) for the higher order schemes (CN, FS, GL) and for the 1st order Backward Euler (BE) the amplitude of oscillations (≈ 12.42) of rear mass shows 10 percent less accuracy compared to CN, FS and GL. For $\Delta t = 0.00005$ Backward Euler (BE) shows better agreement of the amplitude of oscillations (≈ 13.71) of the rear mass to CN, FS, GL. For larger time step, GL is more damped than CN and FS. We use two different meshes (see Fig. 5 and 6) and also we increase the mesh refinement level from level 1 to level 2. Corresponding plots for two different meshes and different mesh refinement levels are given in figure 8 and figure 9 which shows that our solution is almost independent of mesh type and mesh refinement levels. From experimental results, for velocity $1130mm/s$ the structure shows hysteric behavior, but in our simulations no hysteric behavior could be observed so for and resulting frequency of oscillations is $\approx 10Hz$ for applying all the four time stepping schemes mentioned above.

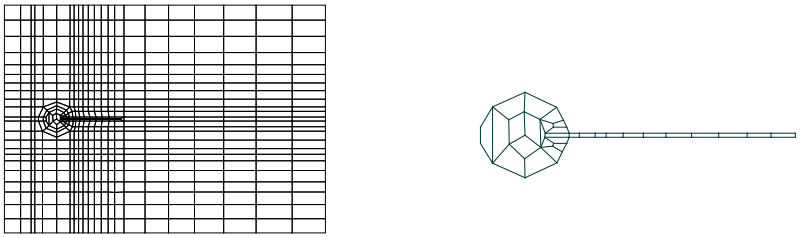

Fig. 5. Coarse mesh1 with 576 elements, 622 nodes and 11308 dof.

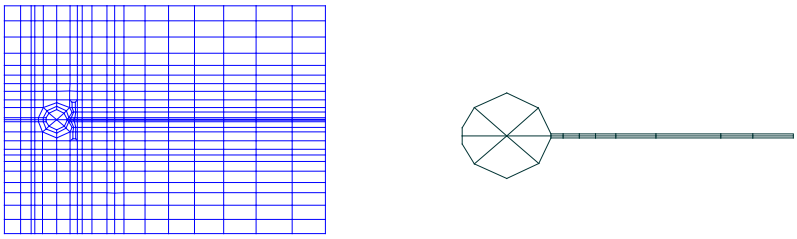

Fig. 6. Coarse mesh2 with 529 elements, 574 nodes and 10407 dof.

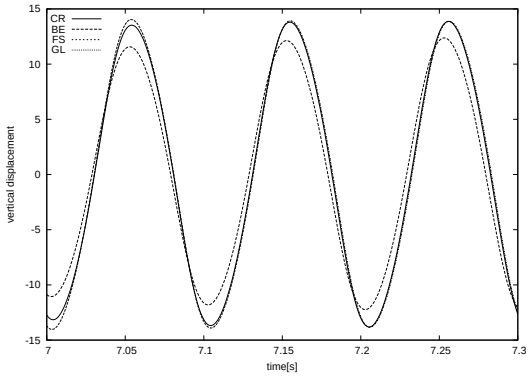

Fig. 7. For $\Delta t = 0.0005$, the amplitude of oscillations of rear mass is almost identical for the different time stepping schemes CN, FS, GL.

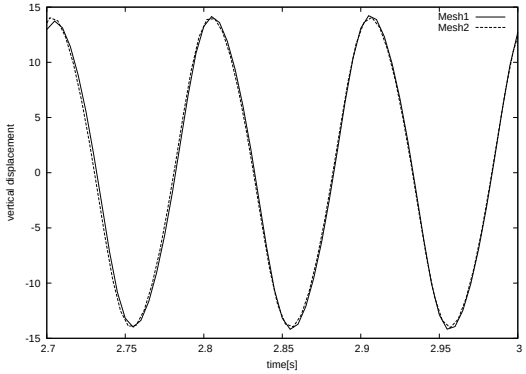

Fig. 8. For the two different meshes, the amplitude of oscillations is almost the same for the Fractional-Step-θ-scheme.

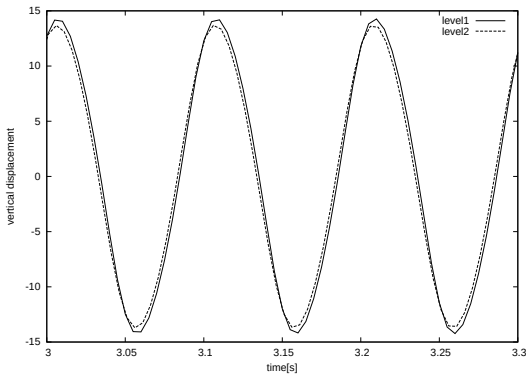

Fig. 9. For refinement level 1 and 2 (mesh1) the amplitude of oscillation is almost identical.

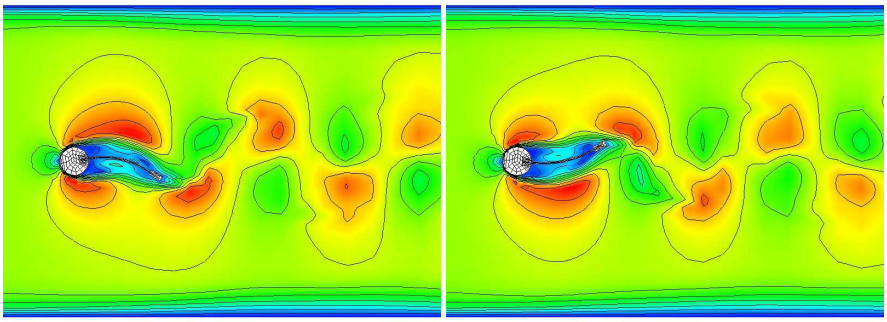

Fig. 10. Snapshots of the vertical displacement of the rear mass with frequency of oscillations $\approx 10Hz$ for $1mm$ thick beam.

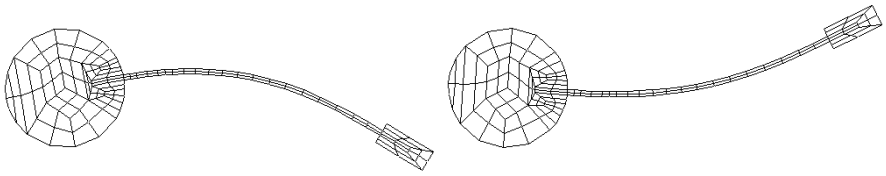

Fig. 11. Zoomed snapshots of the deformed $1mm$ thick beam .

6.2 Results for 0.04mm thick beam

In this test we keep the thickness of the beam $0.04mm$ as described in the experimental set up. The minimum velocity needed to excite the movement of the structure slightly varied from test to test. In our case for velocity $600mm/s$ ($Re \approx 80$) we are able to excite the structure. Frequency of the structure movement increases linearly with the increase of the velocity of the fluid. We used the velocity $600mm/s$ ($Re \approx 80$) at beginning, then switching to $800mm/s$ ($Re \approx 107$) for simplicity, see figure 14 and 15. Figure 12 shows the comparison between experimental versus numerical results of the problem. Figure 13 shows the amplitude of oscillations of rear mass attached to the elastic beam for velocity $1080mm/s$ and the frequency of oscillation observed is $\approx 9.5Hz$. Figure 17 and 18 shows the deformed shape of the beam for velocity $1080mm/s$, and for the velocity $1450mm/s$ the deformation of the elastic beam is even more significant, see figure 19 and 20.

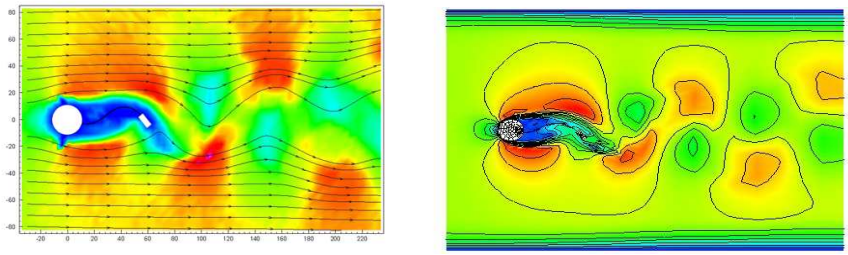

Fig. 12. Experiment from Erlangen (left) and numerical result for velocity $1450mm/s$ (right).

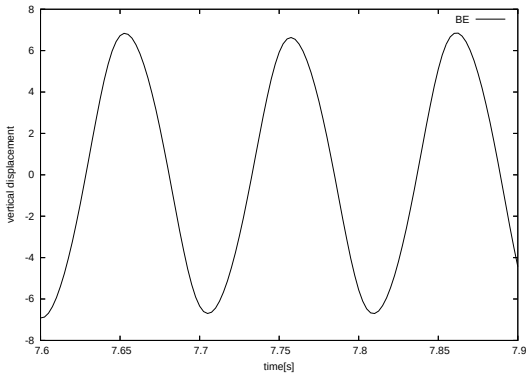

Fig. 13. Frequency of oscillations of the rear mass for velocity 1080 mm/s for the described numerical set up is $\approx 9Hz$.

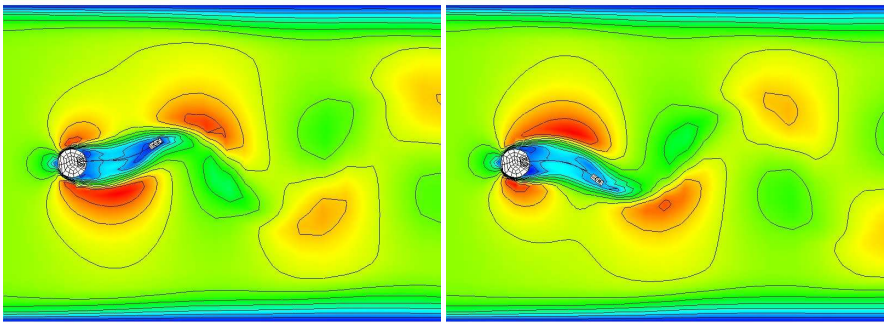

Fig. 14. Snapshots of the vertical displacement of the rear mass with maximum amplitude ≈ 17.0 and frequency $\approx 4.5Hz$ and velocity $800mm/s$.

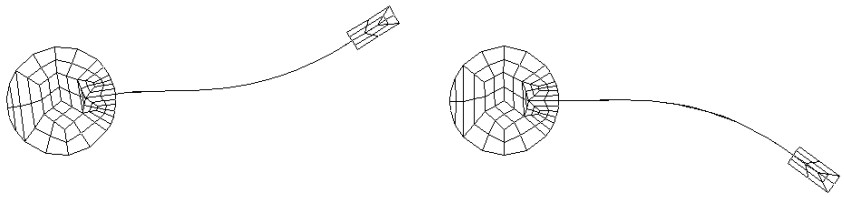

Fig. 15. Zoomed snapshots of the deformed beam for velocity $800mm/s$.

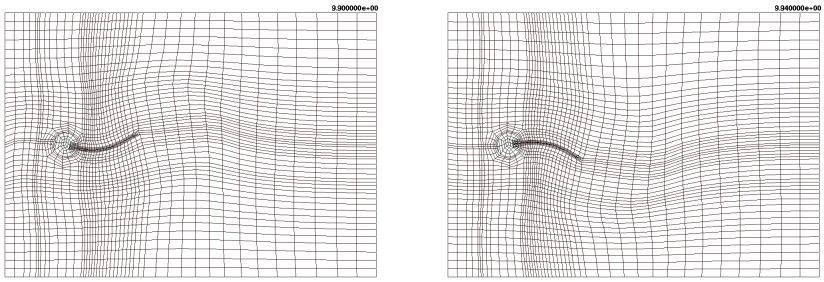

Fig. 16. Snapshot of the complete mesh.

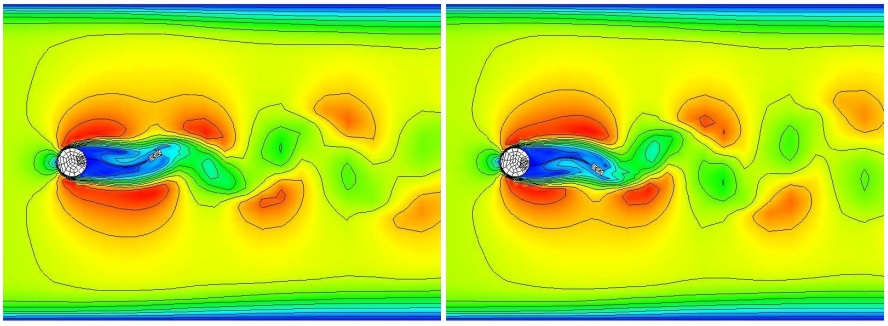

Fig. 17. Snapshots of the vertical displacement of the rear mass for velocity $1080mm/s$.

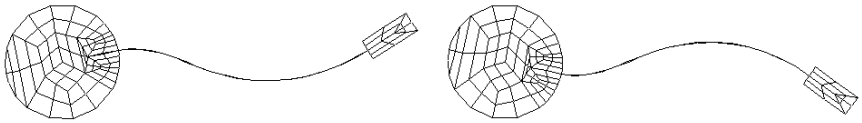

Fig. 18. Zoomed snapshots for deformed thick beam.

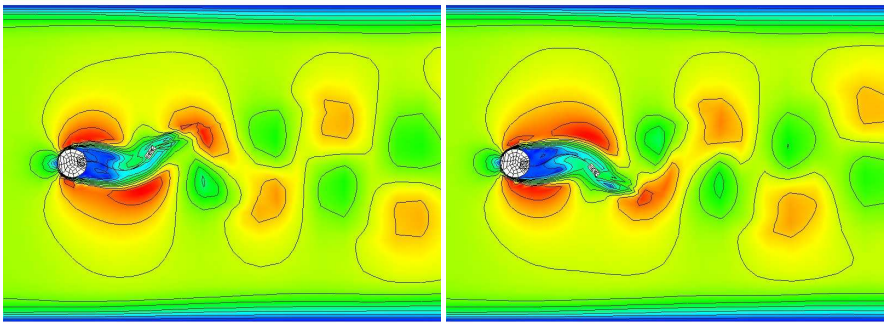

Fig. 19. Snapshots of the vertical displacement of the rear mass and velocity $1450 mm/s$.

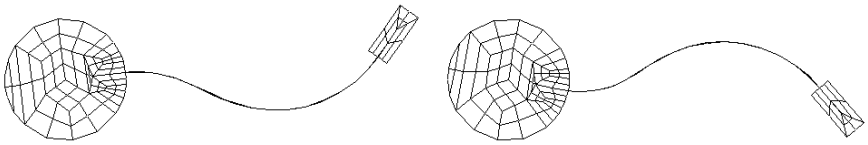

Fig. 20. Zoomed snapshots for the deformed beam.

7 Summary and future developments

We presented a general ALE formulation of fluid-structure interaction problems suitable for applications with finite deformations of the structure and laminar viscous flows. The resulting discrete nonlinear systems arise from the finite element discretization by using the high order Q_2P_1 FEM pair which are solved monolithically via discrete Newton iteration and special Krylov space and multigrid approaches. We applied the Backward Euler, Crank Nicholson,

Fractional-Step-θ-scheme and a new modified Fractional-Step-θ-scheme for time discretization which are numerically examined for several prototypical benchmark configurations.

Results have been given that are obtained from a rigid cylinder in laminar flow. The structure consists of a thin elastic beam attached to the cylinder, which is identified by the center of the cylinder with one grid point. This point constraint effectively fixes the position of the cylinder axis, but still allows the free rotation around this point. At the trailing end of the beam a rear mass is attached. We simulated two cases corresponding to the thickness of the beam to be $1mm$ and $0.04mm$, respectively. Additionally, we present numerical studies on different mesh types. Numerical results are provided for all time stepping schemes which show very reproducible symmetrical two–dimensional swiveling motions. These numerical tests show that the solution is independent of the mesh type and mesh refinement level. Preliminary results for the experimental benchmark configuration are shown to see the qualitative behavior of the elastic beam for a high velocity profile fluid. The next steps regarding better efficiency of the solvers include the development of improved multigrid solvers, for instance of global pressure Schur complement type [6], and the combination with parallel high performance computing techniques in future, particularly towards $3D$ configurations.

8 Acknowledgement

This work is supported by the German Research Association (DFG), Research unit 493, by the Jindrich Necas Center for Mathematical Modeling, project LC06052 financed by MSMT, and by the Higher Education Commission (HEC) of Pakistan. This support is gratefully acknowledged.

9 Reference

1. Arnold, D. N., Boffi, D., and Falk, R. S. *Approximation by Quadrilateral Finite Element*, Math. Comput., 71(239):909-922, 2002.
2. Boffi, D. and Gastaldi, L. *On the Quadrilateral Q2-P1 Element for the Stokes Problem*, Int. J. Numer. Meth. Fluids, 39:1001-1011, 2002.
3. Gresho, P. M. *On the theory of semi-implicit projection methods for viscous incompressible flow and its implementation via a finite element method that also introduces a nearly consistent mass matrix, part 1: Theory*, Int. J. Numer. Meth. Fluids, 11: 587-620, 1990. Press, 1978.
4. Hron, J., Quazzi, A., Turek, S. *A Computational Comparison of two FEM Solvers For Nonlinear Incompressible Flow*, Bansch, E., LNCSE, 87–109, Challenges in Scientific Computing CISC 2002, . Springer, .ISBN 3–540–40887-8, 2002.
5. Rannacher, R. and Turek, S. *A Simple nonconforming quadrilateral Stokes element*, Numer. Methods Partial Differential Equations, 8:97-111, 1992.
6. Turek, S. *Efficient Solvers for Incompressible Flow Problems: An Algorithmic and Computational Approach*, LNCSE 6, Springer-Verlag, 1999.
7. Turek, S., Rivkind, L., Hron, J., Glowinski, R. *Numerical Study of a Modified Time-Steeping theta-scheme for incompressible flow simulations*, Journal of Scientific Computing, 28, 533-547, 2006.

8. Glowinski, R. *Finite element method for incompressible viscous flow*, In: Handbook of Numerical Analysis, Volume IX, Ciarlet,P. G and Lions, J. L., Editors, North-Holland, Amsterdam, pp.3-1176, (2003).
9. Jorge P. Gomes and Hermann Lienhart *Experimental study on a fluid-structure interaction reference test case*, Fluid-Structure Interaction: Modelling, Simulation, Optimisation Lecture Notes in Computational Science and Engineering , Vol. 53, pages 356 - 370 Bungartz, Hans-Joachim; Schäfer, Michael (Eds.) Springer (ISBN: 3-540-34595-7), 2006.
10. Barrett, R. and Berry, M. and Chan, T. F. and Demmel, J. and Donato, J. and Dongarra, J. and Eijkhout, V. and Pozo, R. and Romine, C. and Van der Vorst, H. *Templates for the solution of linear systems: Building blocks for iterative methods*,SIAM Philadelphia, PA 1994.
11. Davis, T. A. and Duff, I. S. *A combined unifrontal/multifrontal method for unsymmetric sparse matrices*,pp.1-19, Vol 25, SACM Trans. Math. Software, 1999.
12. Vanka, S.P. *Implicit Multigrid Solutions of Navier-Stokes Equations in Primitive Variables*, pp.138-158 J. of Comp. Phys.Vol 65, 1985.
13. Bramley, R. and Wang, X. *SPLIB: A library of iterative methods for sparse linear systems* Department of Computer Science, Indiana University, Bloomington, IN, `http://www.cs.indiana.edu/ftp/bramley/splib.tar.gz`. 1997.
14. Turek, S., Schmachtel, R. *Fully coupled and operator-splitting approaches for natural convection flows in enclosures*.International Journal for Numerical Methods in Fluids, pp. 1109-1119, 2002.
15. Hron, J., Turek, S. *A monolithic FEM /Multigrid solver for ALE formulation of fluid-structure interaction with application in biomechanics*, Bungartz, H., –J.;Schfer, M. , Lecture Notes in Computational Science and Engineering, 53, 146–170, Fluid –Structure Interaction –Modelling, Simulation, Optimization, Springer, ISBN 3–540–34595–7, 2006.